Optical properties of remotely doped AlAs/GaAs coupled quantum wire arrays. II. Fermi-edge singularities

T. Mélin[1,2,*] and F. Laruelle[1,†]
[1]*Laboratoire Photonique et Nanostructures, Centre National de la Recherche Scientifique, 196 Avenue Henri Ravera, BP 107, 92225 Bagneux Cedex, France*
[2]*Institut d'Electronique et de Microélectronique du Nord, Centre National de la Recherche Scientifique, Avenue Poincaré, BP 69, 59652 Villeneuve d'Ascq Cedex, France*
(Received 15 October 2001; published 19 April 2002)

We perform low-temperature optical experiments on remotely doped lateral superlattices epitaxially grown on vicinal GaAs substrates. This quantum wire system provides a degenerate electron gas of density $n_s \simeq 8 \times 10^{11}$ cm^{-2} subjected to a tunable one-dimensional periodic potential of amplitude $\simeq 20$ meV and period $\simeq 30$ nm, i.e., at the scale of its Fermi energy ($E_F \simeq 25$ meV) and Fermi wavelength ($\lambda_F \simeq 30$ nm). The enhancement of Fermi-edge singularities in tilted lateral superlattices [T. Mélin and F. Laruelle, Phys. Rev. Lett. **76**, 4219 (1996)] is examined in the framework of the Fano resonance scheme that we recently proposed for two-dimensional systems in presence of alloy disorder [T. Mélin and F. Laruelle, Phys. Rev. Lett. **85**, 852 (2000)]. Including periodic intersubband couplings as extrinsic scatterings in the Fano model, we obtain a nice agreement with experimental data. This thus rules out possible many-body scenarios for the enhancement of Fermi-edge singularities in lateral superlattices, where multiple Coulomb diffusions of Fermi-sea electrons by charged photocreated valence holes would be boosted by the reduced dimensionality.

DOI: 10.1103/PhysRevB.65.195303 PACS number(s): 78.66.−w, 71.10.Ca, 73.21.−b, 71.35.−y

I. INTRODUCTION

Fermi-edge singularities (FES's) refer to the divergence of optical oscillator strength for Fermi-level transitions in a degenerate electron gas (DEG),[1] first identified in the x-ray absorption spectra of simple metals such as Al, Na, and K nearly three decades ago.[2] Mahan[3] and Nozières and De Dominicis[4] explained the FES formation as a result of the presence of the Coulomb potential of charged core holes during the optical experiments. This potential multiply scatters Fermi-sea electrons throughout and along the DEG Fermi surface, which results in power-law divergences at the optical Fermi edges of emission or absorption spectra. Additional points have also been clarified by theories: first the role played by the Anderson infrared catastrophe during optical processes[5] which tends to suppress the optical oscillator strength around Fermi edges and thus reduces the FES power-law divergence exponents as clarified by Nozières *et al.*[4] and, also, the role played by the hole localization and the DEG dimensionality, limiting the observation of FES's to regimes with either strong hole localization or the dimensionality being unity because of phase-space restrictions in Coulomb diffusion processes.[6]

Semiconductor structures have generated much interest in studying FES issues. First, optical experiments can be easily performed by means of photoluminescence (PL) or PL excitation (PLE), generally in the visible range, the role of core holes being played by photocreated minority carriers, i.e., valence holes in the case of a remote doping achieved in the heterostructure conduction band. Also, the semiconductor materials in which DEG's are embedded are *tailorable*, so that specific structures can be designed in order to establish the Coulomb nature of observed FES's and then to test theories with respect to localization and dimensionality issues.

The first observation of a divergent Fermi edge is due to Skolnick *et al.* in 1987 (Ref. 7) in the PL spectrum of an InGaAs/InP quantum well and was attributed to a FES effect owing to the localization of valence holes in the disordered quantum well material. Since then, new experimental situations have been achieved in semiconductor structures with weaker valence hole localization,[8,9] showing that FES's could appear when Fermi-level transitions are brought in close resonance with empty subband excitonic levels. To explain this behavior, a many-body mechanism was proposed on the basis of numerical calculations in the infinite hole-mass approximation,[10] putting forward the efficiency of Coulomb intersubband scattering processes to enhance FES's.

We demonstrated recently[11] that the experimental excitonic enhancement of FES's is rather due to a Fano resonance mechanism[12] involving extrinsic intersubband scattering processes—like alloy disorder—rather than Coulomb ones. Parasitic FES's can thus easily develop in optical spectra due to the presence of empty—and even remote—subbands and to extrinsic intersubband couplings such as disorder. This emphasizes the essential need to determine the detailed band structure and disorder processes from experimental data before the Coulomb origin of FES's can be established. Since these two ingredients can hardly be known from the PL measurements where the FES's are usually observed, it requires that optical absorption data be systematically recorded and analyzed in order to evaluate the weight of extrinsic Fano processes in experiments.

The aim of this paper is to test the relevance of the Fano resonance model to account for the FES's observed in quantum wire arrays known as lateral superlattices (LSL's).[9] Given the paramount importance of the FES topic in reduced dimensionalities, it appears crucial to determine the physical nature of FES enhancements in LSL's from a quantitative analysis of experiments. This makes the scope of the present

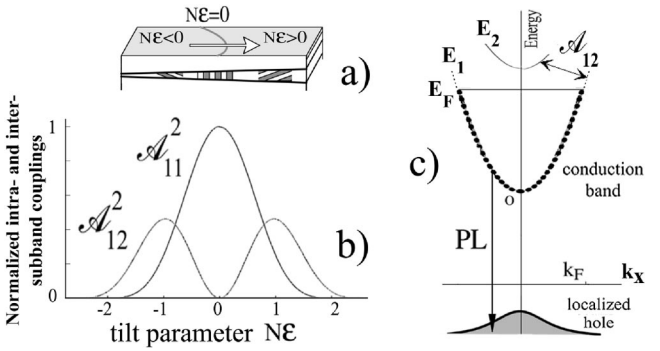

FIG. 1. (a) Schema showing how optical properties are tracked as a function of tilt along a given sample. (b) squared normalized intra- and intersubband couplings $\mathcal{A}_{11}^2$ and $\mathcal{A}_{12}^2$ as a function of $N\varepsilon$. (c) In-plane band structure of a 2D DEG with PL recombinations on localized hole levels. The LSL tilt induces intersubband couplings between states separated $\pm 2\pi/L_x$ along the k_x direction of reciprocal space.

paper, the fabrication and other optical properties of LSL's being extensively described in the preceding paper.[13] We show that experimental FES enhancements are well described by a microscopic Fano theory taking into account the LSL periodic intersubband couplings as extrinsic scattering processes. The quantitative agreement reached with experiments emphasizes the conclusion of Ref. 11 in two dimensions (2D), showing that intersubband scattering processes of extrinsic origin easily predominate experimentally over many-body contributions to FES enhancements.

The paper is organized as follows. After a brief description of the experiments of Ref. 9, we detail the Fano resonance model used in Ref. 11. Fano parameters are then computed, first in the case of random alloy disorder and then in the case of the periodic potential of LSL's. The theory is finally quantitatively compared to experimental data.

II. SAMPLES AND EXPERIMENTS

We perform 2K PL experiments on remotely doped LSL's epitaxially grown on vicinal GaAs substrates with 0.5° miscut. This quantum wire system provides a DEG of density $n_s \simeq 8\times 10^{11}$ cm^{-2} subjected to a tunable 1D periodic potential of amplitude $\simeq 20$ meV and period $L_x = 32$ nm, i.e., at the scale of its Fermi energy ($E_F \simeq 25$ meV) and wavelength ($\lambda_F \simeq 30$ nm).

The sample fabrication and electronic properties of tilted LSL's are described in the preceding paper.[13] We report here only on the FES aspects of the samples[9] and their correlation with tilt-induced periodic intersubband couplings. The LSL tilt originates in flux gradients of effusion cells inside the molecular beam epitaxy growth chamber and thus corresponds to the local relative deviation ε from the nominal AlAs and GaAs fluxes required to cover exactly the LSL terrace during growth cycles.[13] The tilt angle β ($\beta = \epsilon/\alpha$, α being the wafer miscut angle) continuously varies along samples (see Fig. 1). However, this parameter is inappropriate to describe the electronic properties of LSL's. One rather needs to take into account the vertical extension of the envelope wave functions of the 2D electron and hole states E_i and

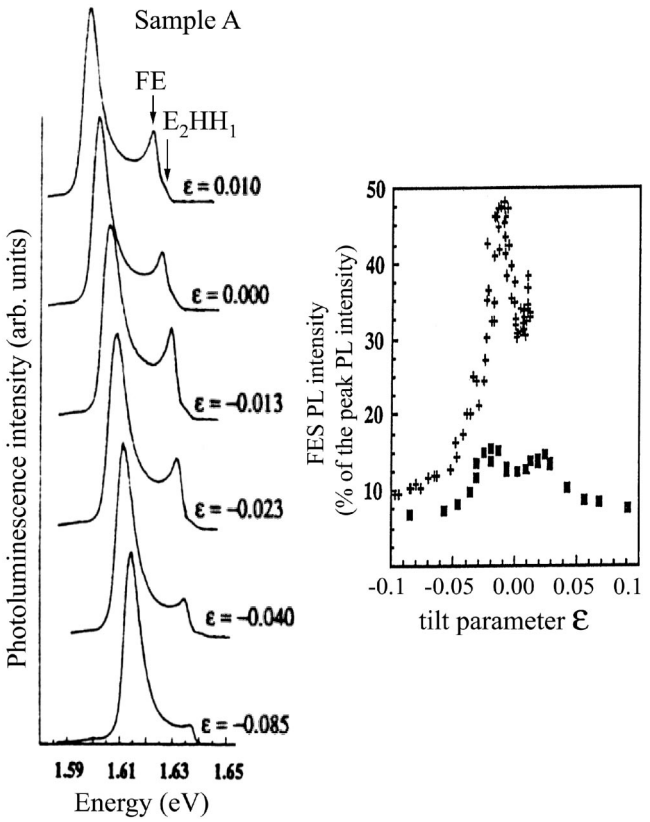

FIG. 2. Left: 2 K PL spectra of sample A ($\Delta = E_{2_X} - E_F = 6.5$ meV) measured when tilt is varied along the sample. Right: FES intensities of samples A and B, normalized with respect to the peak intensity of low wave-vector PL transitions. The camelback behavior is typical of $\mathcal{A}_{12}^2$ in Fig. 1.

HH_i which probe the LSL confinement potential. We use here $N\varepsilon$ as the tilt parameter, N being the LSL thickness in monolayers ($N = 71$ and 55 for samples A and B, respectively). $2\pi N\varepsilon$ corresponds to the phase shift of the LSL confinement potential throughout the N-monolayer-thick LSL.

For nontilted LSL's ($N\varepsilon = 0$), the 1D periodic potential is separable between the [110] (x) and the growth [001] (z) directions. The broken separability between x and z in tilted LSL's ($N\varepsilon \neq 0$) induces periodic intersubband couplings acting between electronic states belonging to subbands with different quantum numbers [see Fig. 1(c) for illustration]. The relative amplitudes of the lowest-index inter- and intrasubband coupling terms $\mathcal{A}_{12}(N\varepsilon)$ and $\mathcal{A}_{11}(N\varepsilon)$ are depicted in Fig. 1. It shows the typical camelback shape of $\mathcal{A}_{12}^2$ as a function of $N\varepsilon$.

Periodic intersubband coupling effects have been found in the PL data of samples A and B in Ref. 9. Their observation is related to the peculiar interplay between the sample DEG densities (and thus Fermi wave vectors $k_F \simeq 0.022$ Å^{-1}) and the wave vector associated with the LSL period $2\pi/L_x \simeq 0.020$ Å^{-1}. This means that Fermi-level electrons populating the first subband E_1 are efficiently coupled with zone-center electrons in E_2 for sufficiently small $\Delta = E_{2_X} - E_F$ energy separations. We reproduce for illustration in Fig. 2 the

raw PL spectra of sample A from Ref. 9 for various tilt parameters. First, the figure shows an enhancement of FES intensities as a function of tilt, with camelback shape variations typical of the $\mathcal{A}_{12}^2$ intersubband coupling parameter (see Fig. 1). These variations occur due to the much greater oscillator strength of E_{2_X} transitions (of excitonic character) compared to $E_1\mathrm{HH}_1$. Second, FES enhancements effects are more pronounced in the case of sample A, correlated to a smaller energy separation $\Delta = 6.5$ meV between E_{2_X} and E_F compared to sample B where $\Delta = 19.5$ meV.[13] These two features demonstrate the presence of periodic intersubband couplings in LSL's. Also, the FES enhancement extremum is obtained for $N\varepsilon = 0.92 \pm 0.14$ and $N\varepsilon = 1.26 \pm 0.06$ for samples A and B, in good agreement with the $N\varepsilon = 1$ value from the square quantum well (QW) model calculations sketched in Fig. 1. However, in the absence of relevant microscopic models, we did not evaluate in Ref. 9 the actual variations of the FES oscillator strength beyond qualitative and phenomenological considerations.

III. FANO RESONANCE MODEL

We here describe in more details the Fano model and calculations relative to Ref. 11. It consists in using the discrete nature of excitonic resonances associated with empty conduction subbands in order to get an analytical description of the interaction between DEG states and empty conduction subbands (see Fig. 3). We thus basically consider a discrete state $|i\rangle$ coupled to a continuum of states $|k\rangle$ by a matrix element W. The coupled system is ''observed'' through transitions onto a third level $|\nu\rangle$, described by a H_{pert} Hamiltonian in the perturbation theory. In our case, the observation is performed by means of photoluminescence spectroscopy. $|\nu\rangle$ therefore represents valence hole states, which we consider of infinite mass for simplicity. In this approximation, the continuum of E_2 states corresponds to the distribution of $E_1\mathrm{HH}_1$ electron-hole pairs, with a population factor given by the Fermi-Dirac distribution of electrons in the E_1 subband. The discrete level $|i\rangle$ is assumed to be the excitonic resonance E_{2_X}. This description therefore considers the Coulomb interaction between valence holes and the empty conduction subband E_2, but neglects any with DEG states filling the first conduction subband E_1.

Fano[12] described analytically the shape of the recombination spectra of the coupled (discrete level+continuum) system onto the level $|\nu\rangle$. Assuming a constant oscillator strength for the continuum in the $W \to 0$ limit and measuring energies with respect to the discrete level transition, the recombination spectrum reads

$$I(E) = \frac{|q+\xi|^2}{1+\xi^2},$$

where ξ denotes a reduced energy value E/Γ. Here q and Γ are the two parameters controlling the recombination line shape. Γ represents the spectral spreading of the discrete state $|i\rangle$ coupled to the continuum of states $|k\rangle$. It equals $\pi W^2 \mathcal{D}$, where $\mathcal{D}$ is the density of states of the continuum. q^2 measures the oscillator strength of the broadened discrete

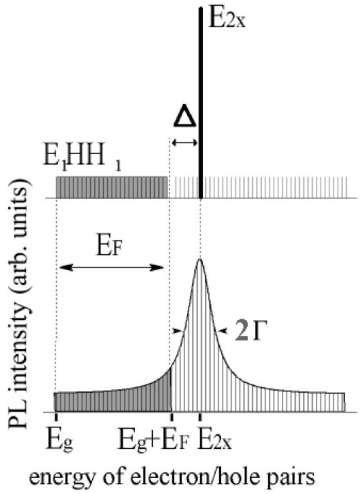

FIG. 3. Fano resonance scheme with zero (top) and nonzero (bottom) intersubband coupling amplitude W. For $W \neq 0$, a singularity appears at the Fermi edge of the optical emission spectrum (dark gray) of the DEG filling the first conduction subband E_1. Parameters are defined in the text.

level for $W \neq 0$, compared to that of the continuum for $W = 0$. It depends on the optical matrix elements $\langle \nu|H_{pert}|i\rangle$ and $\langle k|H_{pert}|i\rangle$ of E_{2_X} and $E_1\mathrm{HH}_1$ by the formula

$$q = \frac{\langle \nu|H_{pert}|i\rangle}{\langle \nu|H_{pert}|k\rangle \pi W \mathcal{D}}.$$

The main feature of Fano's theory was its explanation of the asymmetrical character of x-ray spectra line shapes involving discrete levels.[12] This point originates in the interference between ξ and q terms as the energy is scanned in the above formula. Similar asymmetries have already been reported in optical spectra of semiconductor heterostructures.[14] However, as explained in the following, such effects will not arise in our samples due to specific properties on the W interaction. As seen from Fig. 3, the formation of FES's in optical spectra simply comes from the Fermi-Dirac filling of the Fano profile in the 2D quantum limit (i.e., for a negative reduced Fermi energy ξ_F). The divergent behavior corresponds to the positive slope of the Fano profile at E_F, all the more pronounced with reduced $\Delta = E_{2_X} - E_F$ energy separations. In experimental PL data, FES's, however, only occur when the positive slope from the Fano profile at E_F overcomes the nominal decay of the DEG PL with energy associated with PL recombination on localized valence holes or indirect processes.[15]

In the Fano resonance model, two means thus exist to enhance Fermi-edge singularities in the PL spectrum of a DEG: on the one hand, by putting PL Fermi-level transitions into resonance with E_{2_X} (this was reported experimentally by Chen *et al.*[8] nearly a decade ago) and on the other hand, by increasing intersubband couplings (or equivalently the Fano parameter Γ) at fixed $\Delta = E_{2_X} - E_F$ energy separations (we demonstrated this point quantitatively in 2D systems with a random alloy disorder).[11]

Our purpose is to show that the Fano scheme also corresponds to the case of LSL's, where periodic intersubband couplings generated by tilt act as the extrinsic intersubband scattering necessary for the Fano process. To do so, we successively compute the Fano parameters (i) in the case of alloy disorder which accounts for 2D DEG's embedded in ternary-alloy materials like $Al_xGa_{1-x}As$, but also for samples A and B in the limit of large tilt values ($N\varepsilon \to \infty$), and (ii) in the case of periodic intersubband couplings in tilted LSL's. The theory is then compared to experiments.

IV. CALCULATION OF ALLOY-DISORDER FANO PARAMETERS

In MBE-grown ternary alloys $A_xB_{1-x}As$ such as AlGaAs or GaInAs alloys, potential fluctuations arise from the random possibility of finding an atom A or B on a given site. The alloy can be described as a mean crystal $A_{\langle x\rangle}B_{\langle 1-x\rangle}As$ of mean potential $xV_A+(1-x)V_B$, with a potential fluctuation on each position $\mathbf{R}_i$ given by[16]

$$h_i = f_i[V_A(\mathbf{r}-\mathbf{R}_i) - V_B(\mathbf{r}-\mathbf{R}_i)],$$

where $V_A(\mathbf{r})$ and $V_B(\mathbf{r})$ denote the potentials of species A and B, f_i equals $1-x$ $(-x)$ with a probability x $(1-x)$. This fluctuation couples states $(1,\mathbf{k})$ and $(2,\mathbf{k}')$ belonging to the first and second subbands E_1 and E_2 and with respective in-plane wave vectors $\mathbf{k}$ and $\mathbf{k}'$. Using the decomposition of $(1,\mathbf{k})$ and $(2,\mathbf{k}')$ onto their envelope functions ϕ_1 and ϕ_2 and on their periodic Bloch wave function $u_c(\mathbf{r})$, the coupling amplitude equals

$$h_i(1,\mathbf{k},2,\mathbf{k}') = \Omega_0 \frac{\delta V}{S} f_i e^{(\mathbf{k}'-\mathbf{k})\cdot\mathbf{R}_i} \int \phi_1(z)\phi_2(z)dz,$$

where Ω_0 denotes the crystal unit cell and with

$$\delta V = \frac{1}{\Omega_0}\int_{\Omega_0} [V_A(\mathbf{r}) - V_B(\mathbf{r})]|u_c|^2(\mathbf{r})d^3\mathbf{r}$$

(δV is the conduction band-gap offset between pure *AAs* and *BAs* materials).

Taking into account the combination $\Sigma_{k'}\Phi(\mathbf{k}')(2,\mathbf{k}')$ for the excitonic level E_{2_X}, one gets

$$h_i(1,\mathbf{k},E_{2_X}) = \Omega_0 \frac{\delta V}{S}\sum_{k'} f_i \Phi(\mathbf{k}') e^{(\mathbf{k}'-\mathbf{k})\cdot\mathbf{R}_i} \int \phi_1(z)\phi_2(z)dz.$$

This coupling is zero, when averaged over all positions $\mathbf{R}_i$, but its squared value—which enters the Fano formula—is nonzero:[16]

$$\langle |h_i(1,\mathbf{k},E_{2_X})|^2\rangle = \Omega_0^2 \frac{\delta V}{S}^2 \frac{1}{\Omega_0} x(1-x)\int \phi_1^2(z)\phi_2^2(z)dz.$$

In the approximation of a square QW of width L_z, we obtain finally

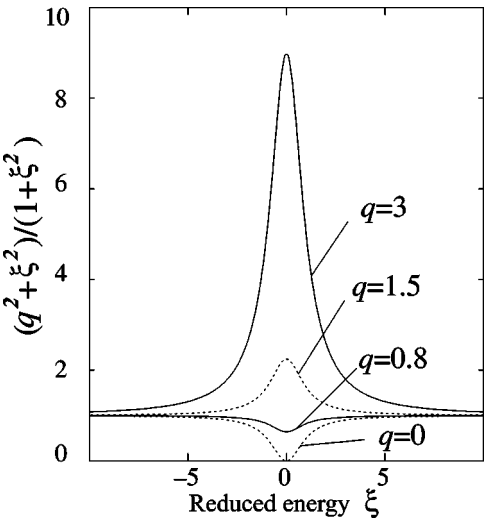

FIG. 4. Fano photoluminescence profiles for various q values plotted as a function of the reduced energy ξ.

$$W^2 = \langle |h_i(1,\mathbf{k},E_{2_X})|^2\rangle = \frac{\Omega_0 \delta V^2}{S} x(1-x)\frac{1}{L_z}$$

and the Fano formula becomes

$$I(E) = \frac{q^2+\xi^2}{1+\xi^2},$$

with a resonance broadening parameter Γ given by

$$\Gamma = \frac{m}{\hbar^2}\Omega_0(\delta V^2)x(1-x)\frac{1}{L_z}.$$

We report for illustration in Fig. 4 Fano profiles for various q values, as a function of the reduced energy ξ.

The validity of the Fano scheme has been demonstrated in Ref. 11 in the case of $Al_xGa_{1-x}As$ remotely doped QW's. A linear increase has been found for the excitonic resonance broadening parameter Γ extracted from measured Fano profiles in the range of alloy content $2.3\% \leqslant x \leqslant 7.1\%$. A quantitative agreement has been also reached on the basis of the Γ formula mentioned above. For this purpose, one also needs to take into account the broadening of the Fano continuum by intrasubband coupling terms induced by the alloy disorder. In the square QW approximation, this contribution reaches exactly $3\Gamma/2$, thus inducing a total broadening parameter $5\Gamma/2$ for the excitonic resonance E_{2_X}. The measured value (0.063 meV/aluminum % in the QW) falls in good agreement with the predicted one (0.054 meV/%), using a $m^* = 0.07m_0$ electron mass.[11] This means that most of the physics has been captured by our model. However, we mention several points, claiming for a more sophisticated modelization. First, the spin quantum number has been explicitly ruled out of our model for sake of simplicity. This should be properly taken into account, since no spin flip is allowed strictly speaking in alloy scattering processes. Doing so will strongly complicate the model, since one then requires a suitable description of the continuum E_1HH_1 and the discrete state E_{2_X} with respect to valence hole (spin) states, which is

nontrivial. One may also expect additionnal corrections due to the E_2HH_1 continuum of states starting a few meV above the excitonic resonance E_{2_X} and to residual alloy-correlation effects which we neglected.

The next sections are devoted to intersubband couplings in lateral superlattices. These couplings superimpose onto residual disorder and alloy-disorder contributions already present in highly tilted ($|N\varepsilon| \gg 1$) LSL's. When needed, we will therefore fix as constant the alloy contribution in the analysis and use its 2D value $\Gamma_0 = 0.6$ meV known experimentally from our work on $Al_xGa_{1-x}As$ QW's.[11]

V. CALCULATION OF FANO PARAMETERS IN TILTED LATERAL SUPERLATTICES

In tilted LSL's, the 1D periodic intersubband potential couples states $(1,\mathbf{k})$ and $(2,\mathbf{k}')$ with $k_x' - k_x = \pm 2\pi/L_x$ and $k_y' - k_y = 0$. Because $k_F \simeq 2\pi/L_x$, Fermi-level states oriented along k_x can get efficiently coupled to zone-center states of E_{2_X}. On the other hand, Fermi-level states oriented along k_y are coupled to $(\pm 2\pi/L_x, 2\pi/L_x)$ states in the exciton wave function, i.e., with a negligible efficiency due to the relatively small k-space extension of E_{2_X} ($1/a_B \simeq 0.01$ Å^{-1}) compared to k_F.

To demonstrate this more quantitatively, we use a quasi-2D description of E_{2_X}:

$$|E_{2_X}\rangle = \frac{2\pi}{L}\frac{1}{\sqrt{2\pi}}\sum_{k'}\frac{2\alpha_B^2}{(\alpha_B^2+k'^2)^{3/2}}(2,\mathbf{k}'),$$

where L denotes the sample length used for 2D plane-wave normalization and α_B the exciton inverse Bohr radius $1/a_B$. For an intersubband potential $V_{12}\cos(2\pi x/L_x)$, we calculate the Fano parameter $\Gamma_{(2\pi/L_x,0)}$ corresponding to a *constant* intersubband coupling between E_{2_X} and Fermi-level electrons in the k_x direction. It equals

$$\Gamma_{(2\pi/L_x,0)} = 2\pi m^* a_B^2 V_{12}^2/\hbar^2.$$

In the k_y direction, Fermi-level electron states $(0,\pm k_F)$ couple to states $(2,\mathbf{k}') = (\pm 2\pi/L_x, \pm k_F)$ of the exciton wave function $|E_{2_X}\rangle$. Since $2\pi/L_x \simeq k_F \simeq 2\alpha_B$, the associated Fano parameter $\Gamma_{(0,2\pi/L_x)}$ would be reduced compared to $\Gamma_{(2\pi/L_x,0)}$ by a factor $\simeq (1+2^2+2^2)^3 = 9^3$. This means that Fano formulas do not rigorously apply to describe experiments in LSL's, since the coupling W is not constant between the continuum states and the discrete level.[12] To circumvent this, we use as a first approximation a Fano description with a mean Γ parameter obtained by the average of individual $\Gamma_{(k_x,k_y)}$ values along the DEG Fermi surface. A numerical evaluation gives

$$\langle\Gamma\rangle_{LSL} \simeq 0.17 \times 2\pi m^* a_B^2 V_{12}^2/\hbar^2.$$

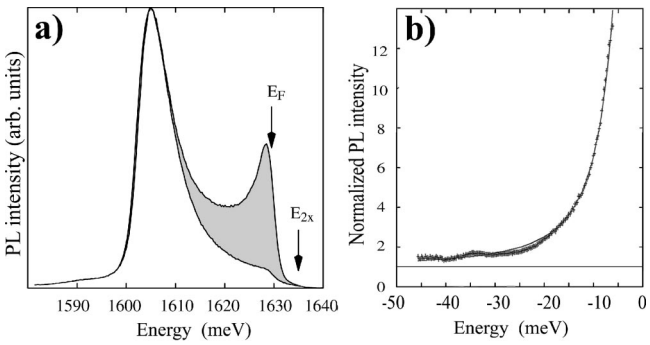

FIG. 5. (a) PL spectra of sample A ($N\varepsilon = 1$) and of sample B ($|N\varepsilon| \to \infty$). Data from sample B have been rigidly energy shifted and normalized so that low wave-vector PL transitions of both samples coincide in this graph for the sake of clarity. Fermi-level transitions and E_{2_X} are indicated by arrows. (b) PL data of sample A normalized by the reference spectrum of sample B, and fitted by a Fano profile with $\Gamma = 3.2$ meV and $q = 7.5$. E_{2_X} is taken as the origin of energies. The horizontal line (unity normalized PL intensity) corresponds to raw PL intensities which would be unenhanced in the Fano process. This graph shows that Fano processes due to periodic intersubband couplings for $N\varepsilon = 1$ also enhance low wave-vector transitions in sample A.

VI. EXPERIMENTAL DETERMINATION OF FANO PARAMETERS IN LATERAL SUPERLATTICES

We evaluate q and Γ values for sample A in the regime of maximized intersubband couplings ($N\varepsilon = 1$). The PL spectrum of sample A is reproduced in Fig. 5(a), with arrows showing the energy of Fermi-level transitions and E_{2_X} as determined from magneto-optical experiments.[17] A first estimate of q and Γ for $N\varepsilon = 1$ can be obtained as follows. Γ is taken as the E_{2_X} half width at half maximum, which can be obtained by raising the DEG temperature under strong optical illumination. This gives $\Gamma \simeq 3.1$ meV. To evaluate q, one notices that in a Fano line shape, the continuum emission intensity gets doubled when $q = \Delta/\Gamma$. This allows us to estimate $q \simeq 5.3$ by comparison between sample A for $N\varepsilon = 1$ and sample B for $N|\varepsilon| \gg 1$ taken as a reference spectrum.

An alternative determination of q and Γ consists in a direct fit to the Fano profile following Ref. 11. A normalization of the PL line shape is required to remove the nominal PL variations corresponding to localization and indirect PL processes. For this purpose, we use the PL spectrum of sample B in the $|N\varepsilon| \gg 1$ limit (sample A is discarded since it already displays some Fano effect for $|N\varepsilon| \gg 1$ due to alloy disorder because of its relatively small $\Delta = 6.5$ meV parameter). The normalized PL data from sample A in $N\varepsilon = 1$ is displayed in Fig. 5(b) and fitted by a Fano profile with parameters $\Gamma = 3.3$ meV and $q = 7.8$. In this figure, the continuum PL intensity in absence of FES enhancement set to unity (horizontal line). This shows that the spreading of the excitonic resonance E_{2_X} already enhances zone-center transitions in sample A for $N\varepsilon = 1$. It explains the difference between the fitted q value and the one we estimated using the criterium of a doubled PL intensity for $q = \Gamma$, while both estimated and fitted Γ parameters fall in good agreement.

Substracting $\Gamma_0 = 0.6$ meV to account for alloy-disorder scatterings,[11] we obtain $\langle\Gamma\rangle_{LSL} \simeq 2.5$ meV. From the formula established for $\langle\Gamma\rangle_{LSL}$, we extract the associated value for the intersubband coupling amplitude $2V_{12} \simeq 10$ meV and finally the peak-to-peak conduction-band amplitude of the LSL potential $2V_{1D} \simeq 15$ meV using the tilt model of Ref. 18. This value falls in quantitative agreement with the $\simeq 20$ meV expected value in samples A and B. This demonstrates that periodic intersubband couplings control the FES formation through a Fano resonance.

VII. TILT DEPENDENCE OF FERMI-EDGE SINGULARITIES IN LATERAL SUPERLATTICES

We discuss here the variations of the enhancement of FES's with tilt in lateral superlattices (camelback profiles in Fig. 2). To do so, one needs to find a suitable model to describe the variations of Γ and q parameters with $N\varepsilon$.

As for the Γ Fano parameter, we adopt a model summing the alloy contribution $\Gamma_{alloy} \simeq 0.6$ meV (Ref. 11) and the LSL one $\langle\Gamma\rangle_{LSL}$. The variations of $\langle\Gamma\rangle_{LSL}$ with $N\varepsilon$ are then described using the square QW tilt model of Ref. 18 and the LSL Fano parameter $\langle\Gamma\rangle_{LSL} \simeq 2.5$ meV found for $N\varepsilon \simeq 1$ in sample A. Since Γ only depends on alloy scattering and periodic intersubband couplings, we can expect similar values for Γ in both samples A and B which were grown under identical MBE conditions.

The estimation of q values with tilt is not so straightforward, even if q is expected to vary as $1/W$ at first sight. In fact, q also depends on wave function overlaps through the ratio of the oscillator strength of E_{2_X} and $E_1\mathrm{HH}_1$. It is therefore quite sensitive to small geometrical fluctuations from sample to sample. q values should therefore differ from sample A to sample B, due to the different LSL thicknesses. Also, the wave function of localized hole levels varies with tilt and, consequently, affects both E_{2_X} and $E_1\mathrm{HH}_1$ oscillator strengths. Variations of q with tilt are therefore not predictable *a priori* and must be evaluated from experiments.

The analysis of the FES enhancement with tilt can be made as follows in the case of sample A. We extract q from the data of Fig. 2 for $N\varepsilon \to \infty$. In this limit, FES intensities get already enhanced by the alloy disorder for sample A due to a relatively small $\Delta = E_{2_X} - E_F$ value, while this Fano process is clearly unefficient for sample B due to the much larger $\Delta = 19.5$ meV spacing. Assuming that valence hole localization processes are similar in both samples, this allows us to fit $q \simeq 8$ from the comparison between the FES intensity values of samples A and B in the $N\varepsilon \to \infty$ limit. As we already estimated $q \simeq 7.8$ for sample A for $N\varepsilon = 1$, this suggests that q hardly varies with tilt. We therefore adopt $q = 8$ for all $N\varepsilon$ tilt values. This allows to calculate the FES enhancement as a function of $N\varepsilon$ in the case of sample A (Fig. 6).

Before commenting on Fig. 6, we focus on sample B. As explained above and in contrast with sample A, the q Fano parameter cannot be extracted from optical data in the $N\varepsilon \to \infty$ limit due to the low efficiency of alloy-disorder Fano processes for sample B. A fit from experimental data as a function of $N\varepsilon$ is therefore needed to evaluate q. To do so, we follow the case of sample A and take q as independent of $N\varepsilon$. Using the same Γ value variations as for sample A, the best fit to the FES enhancement as a function of tilt is found taking $q = 11.5$. It is reproduced in Fig. 7.

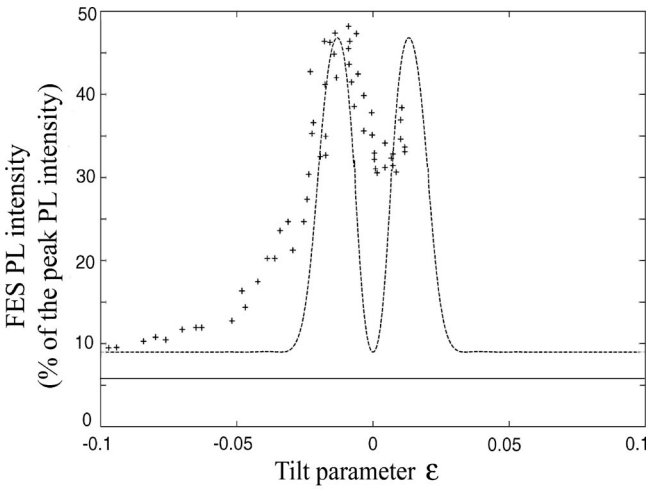

FIG. 6. Points: FES enhancement with tilt for sample A (from Fig. 2). PL intensities are normalized by the peak intensity of low wave-vector PL transitions. Lines: calculated FES intensities using $\Delta = 6.5$ meV, $q = 8$, $\Gamma_{alloy} = 0.6$ meV, and $\langle\Gamma\rangle_{LSL} = 2.5$ meV for $N\varepsilon = 1$ (see text). The horizontal line corresponds to unenhanced PL intensities.

VIII. RESIDUAL FES ENHANCEMENTS FOR $N\varepsilon = 0$

As can be seen from the calculations, the major disagreement of the present theory with experimental data is that it does not account for the experimental enhancement of FES intensities at $N\varepsilon = 0$ for both samples. Indeed, in the framework of our model, periodic intersubband coupling terms vanish for $N\varepsilon = 0$, so that intersubband scattering processes only stem from the alloy disorder in first approximation, and the FES intensity should consequently take the same value as in its $N\varepsilon \to \infty$ limit. As seen from Figs. 6 and 7, experimental data reveal on the contrary a strong residual FES enhancement for $N\varepsilon = 0$, reaching $\simeq 0.6$ times the maximum $N\varepsilon = 1$ FES enhancement for both samples A and B. This re-

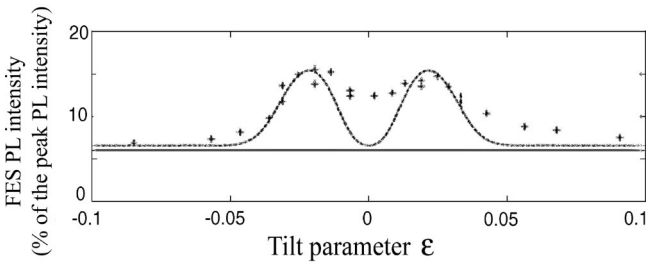

FIG. 7. Points: FES enhancement with tilt for sample B (from Fig. 2). PL intensities are normalized by the peak intensity of low wave-vector PL transitions. Lines: calculated values using the same Γ Fano parameter variations as for sample A and $q = 11.5$ (see text). The horizontal line corresponds to unenhanced PL intensities.

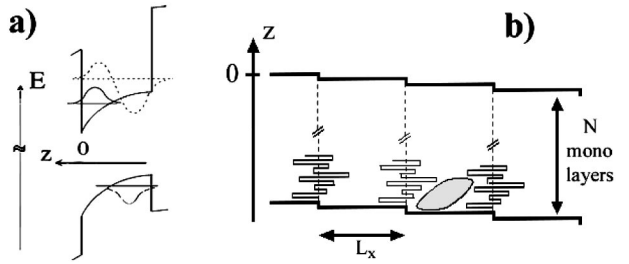

FIG. 8. (a) Left: asymmetric 2D confinement of electron and hole states induced by remote doping. (b) Schematical LSL side view in the (x,z) plane showing the disorder of the terrace step array, together with a hole state (shaded area) localized within one LSL terrace.

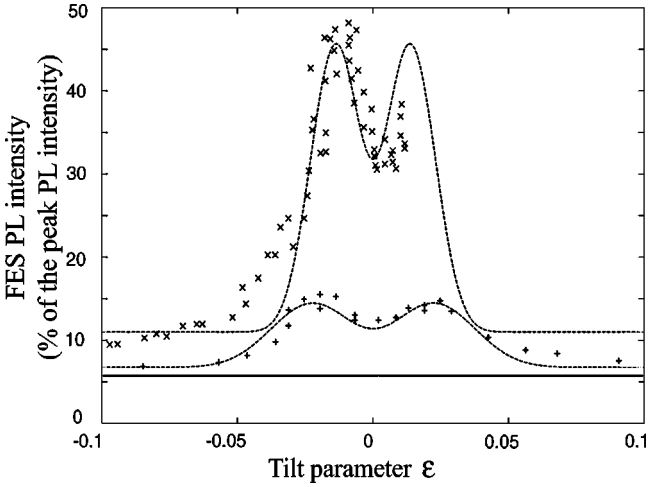

FIG. 9. FES enhancement with tilt in samples A and B (points). PL intensities are normalized by the peak intensity of low wave-vector PL transitions. Fits (lines) correspond to $\Gamma_{alloy}=0.6$ meV and $\langle\Gamma\rangle_{LSL}=2.5$ meV for $N\varepsilon=1$. Constant $q=11$ and $q=16$ values are used, respectively, for samples A and B. A Gaussian convolution of $\Delta N\varepsilon=0.5$ standard deviation is introduced.

sidual enhancement cannot be explained by tilt gradient effects within the laser probe on the sample, the experimental accuracy on the determination of ε being better than 5×10^{-4}.

We propose here an explanation of the FES enhancements in $N\varepsilon=0$ LSL's by taking into account the *finite* localization length of photocreated valence hole states.[19]

Holes are indeed strongly confined, both in the growth direction due to the electrostatic potential associated with the DEG and remote ionized dopants, leading to a few nm z extension, and also in the DEG plane, where they easily localize within one LSL period[13] owing to their relatively large effective mass. Hole states are thus very sensitive to the LSL step array disorder.[20,21] This is sketched in Fig. 8, showing that localized hole states can take a tilted geometry in presence of the step array disorder, even for $N\varepsilon=0$. In PL experiments, the population of photocreated valence carriers thus adopts some tilt-angle distribution, with a standard deviation $\Delta N\varepsilon$ necessarily staying less than unity, because holes are localized within *one* LSL terrace.[13]

We speculate that the hole tilt distribution finds its counterpart in the electronic description of E_{2_X} states, mainly because the hole tilt occurs at a spatial scale comparable with the E_{2_X} exciton Bohr radius. This appears as a dephasing term associated with E_{2_X} in the calculation of the intersubband coupling amplitude $\mathcal{A}_{12}(N\varepsilon)$ and, consequently, to a tilt-convolution effect in PL experiments.

To check for this, we display in Fig. 9 the experimental FES data for samples A and B, fitted by a Fano model using $\Gamma_{alloy}=0.6$ meV, $\langle\Gamma\rangle_{LSL}=2.5$ meV for $N\varepsilon=1$, and constant $q=11$ and $q=16$ values for samples A and B, respectively. A nice overall agreement is obtained with experimental data from both samples by taking a Gaussian tilt-convolution effect of standard deviation $\Delta N\varepsilon=0.5$. This value is less than unity, and thus consistent with the hypothesis of a tilt distribution for valence hole states, as explained above. Also, as holes are localized within $N\simeq25$ monolayers in the growth (z) direction, the measured $\Delta N\varepsilon=0.5$ value corresponds to a standard deviation $\Delta\varepsilon\simeq0.02$ per monolayer. This rough estimate is of the order of magnitude of the standard deviation expected in practice for the coverage ratio ε of each terrace during the molecular beam epitaxy of the LSL, because of the experimental uncertainty on the shutter movements of aluminum and gallium sources in the growth chamber. The above arguments therefore strongly support our explanation of residual FES enhancements in $N\varepsilon=0$ lateral supperlattices in terms of the lateral superlattice disorder.

IX. CONCLUSION

In conclusion, we have shown that the excitonic enhancement of Fermi-edge singularities observed in tilted LSL's is successfully explained by a Fano resonance mechanism taking into account the LSL periodic intersubband coupling as extrinsic scattering processes. This shows that the 1D regime of many-body Fermi-edge singularities[6] is not obtained in LSL's, in spite of the low dimensionality of these coupled QWR arrays. This claims for experiments in a regime of smaller carrier densities and/or stronger 1D confinement amplitudes. From a more general point of view, the work presented in the present paper emphasizes the conclusion of Ref. 11, showing that extrinsic scatterings can easily create parasitic (i.e., non-Coulomb) Fermi-edge singularity effects in optical spectra of degenerate electron systems. We stress that Fano mechanisms should *always* be carefully evaluated in experimental data before assigning observed Fermi level divergences to many-body edge singularities. On the one hand, because semiconductor structures are by essence multisubband structures, so that Fano effects are likely to occur even if achieved degenerate electron gases only populate the first subband of the structures. On the other hand, because parasitic FES effects already appear in low-disorder MBE-grown heterostructures as shown in Ref. 11, they should be drastically boosted in structures with greater disorder.

ACKNOWLEDGMENTS

We are indebted to F. Petit, P. Denk, F. Lelarge, A. Cavanna, R. Planel, C. Tanguy, B. Jusserand, Y.M. Niquet, C. Delerue, G.E.W. Bauer, M. Potemski, and B. Etienne for stimulating discussions. This work was partially supported by DRET and a SESAME grant of the Région Ile de France.

*Electronic address: melin@isen.iemn.univ-lille1.fr

†Present address: Optoplus, Alcatel R&I, Route de Nozay, F-91460 Marcoussis, France.

[1] See, e.g., G.D. Mahan, *Many Particle Physics* (Plenum, New York, 1990).

[2] For a review, see P.H. Citrin, G.K. Wetheim, and M. Schlüter, Phys. Rev. B **20**, 3067 (1979).

[3] G.D. Mahan, Phys. Rev. **153**, 882 (1967).

[4] P. Nozières and C.T. De Dominicis, Phys. Rev. **178**, 1097 (1969).

[5] P.W. Anderson, Phys. Rev. Lett. **18**, 1506 (1967).

[6] See, e.g., P. Nozières, J. Phys. I **4**, 1275 (1994); K. Ohtaka and Y. Tanabe, Phys. Rev. B **39**, 3054 (1989) and references therein.

[7] M.S. Skolnick, J.M. Rorison, K.J. Nash, D.J. Mowbray, P.R. Tapster, S.J. Bass, and A.D. Pitt, Phys. Rev. Lett. **58**, 2130 (1987).

[8] W. Chen, M. Fritze, W. Walecki, A.V. Nurmikko, D. Ackley, J.M. Hong, and L.L. Chang Phys. Rev. B **45**, 8464 (1992).

[9] T. Mélin and F. Laruelle, Phys. Rev. Lett. **76**, 4219 (1996).

[10] J.F. Mueller, Phys. Rev. B **42**, 11 189 (1990); P. Hawrylak, *ibid.* **44**, 6262 (1991).

[11] T. Mélin and F. Laruelle, Phys. Rev. Lett. **85**, 852 (2000).

[12] U. Fano, Phys. Rev. **124**, 1866 (1961).

[13] T. Mélin and F. Laruelle, preceding paper, Phys. Rev. B **65**, 195302 (2000).

[14] C.P. Hopfeld, F. Löser, M. Sudzius, K. Leo, D.M. Whittaker, and K. Köhler, Phys. Rev. Lett. **81**, 874 (1998).

[15] S.K. Lyo, E.D. Jones, and J.F. Klem, Phys. Rev. Lett. **61**, 2265 (1988).

[16] See, e.g., G. Bastard, *Wave-Mechanics Applied to Semiconductor Structures* (Les Editions de Physique, Les Ulis, France, 1988).

[17] T. Mélin, Ph.D. thesis, Ecole Polytechnique, 1998.

[18] T. Mélin and F. Laruelle, Surf. Sci. **361/362**, 762 (1996).

[19] The analytical Fano resonance model described in Sec. III remains nonetheless valid to describe FES enhancements beyond the infinite hole mass approximation, because the localization length and energy for valence carriers are smaller than the conduction degenerate electron gas Fermi wave vector and Fermi energy. This appears clearly from Ref. 11, where the Fano profile is found after normalization of raw PL data, in order to account for the nominal decay of the PL oscillator strength with energy due to the finite localization length of photocreated valence carriers.

[20] F. Lelarge, Z.Z. Wang, A. Cavanna, F. Laruelle, and B. Etienne, Europhys. Lett. **39**, 97 (1997).

[21] On the contrary, this does not apply to electron gas states, which probe the periodic component of the LSL potential: F. Lelarge, F. Laruelle, and B. Etienne, Europhys. Lett. **40**, 213 (1997).